32.4 An Electronically Tunable Multi-Frequency Air-Coupled CMUT Receiver Array with sub-100μPa Minimum Detectable Pressure Achieving a 28kb/s Wireless Uplink Across a Water-Air Interface

Ajay Singhvi, Aidan Fitzpatrick, Amin Arbabian

Stanford University, Stanford, CA

Oceans play a critical role in our ecosystem – they regulate weather and global temperature, serve as the largest carbon sink and the greatest source of oxygen. Maintaining ocean health is of paramount importance and has led to the emergence of the "Internet of Underwater Things (IoUT)" with intelligent sensors being deployed for aquaculture, environmental monitoring, surveillance, and exploration. Given that RF and optical signals are heavily attenuated in water, and ultrasound (US) – which has favorable propagation underwater – faces a large water-air interface loss (~65dB), deep underwater sensing nodes most often communicate data via ultrasonic links to surface buoys, which then use RF to relay data to a remote station. However, such relay-based water-to-air networking solutions are cost and infrastructure intensive, with the inflexibility of anchored buoys prohibiting operation at scale. Wireless, cross-medium communication approaches that do not require intermediary relays would enable large-scale deployment of next-generation IoUT sensors. Previously, laser Doppler vibrometers (LDV) [1] and mm-wave radars [2] have been used to remotely detect displacements on the water surface caused by impinging US waves but suffer from poor sensitivity and low data rates.

In this work, we propose remote US detection in air by using highly sensitive, air-coupled capacitive micromachined ultrasound transducer (CMUT) arrays to overcome the large water-air interface loss. CMUTs, like other MEMS sensors, have an inherent sensitivity-bandwidth tradeoff that directly impacts the SNR and data rates of US links. In prior work [3], increasingly complex CMUT architectures have been proposed to provide a balance between sensitivity and bandwidth, but result in lower reliability and higher fabrication cost, time, and effort. Instead, we exclusively employ electronic tuning knobs – bias voltage and negative capacitance – to independently program the resonance frequency of each element in an array of identical, conventional vacuum CMUT elements that are easier to fabricate at scale. This allows us to synthesize a wideband response across the CMUT array without any drop in sensitivity, thereby overcoming the fundamental sensitivity-bandwidth barrier and demonstrating a noise equivalent pressure (NEP) that is >1000× lower than state-of-the-art water-to-air US links while still achieving a data rate of 28 kb/s – the highest demonstrated by acoustic water-to-air links [1,2].

Figure 32.4.1 shows the system block diagram. It includes an 8-element linear vacuum CMUT array and a chip that has an 8-channel charge pump and analog front-end (AFE). The CMUT elements need to be biased with a high DC (pull-in) voltage for efficient electro-mechanical conversion. This voltage, which also governs CMUT resonance frequency, is generated by a 17-stage charge pump, with a closed-loop mechanism to maintain a stable, low-ripple programmable output. It drives a purely capacitive load, with the design optimized to minimize rise time while meeting the area and power budget [4] and uses 4-phase voltage doublers [5] as building blocks to minimize reversion losses. To reduce any load current requirements, the closed-loop operation is implemented by using a custom high voltage capacitor divider (C_{HV1}, C_{HV2}) with periodic reset via SW_{RST} (implemented using a 5V MOS switch) to provide a feedback voltage, V_{FB} which is compared against a desired reference voltage, V_{REF} using a continuous time comparator. The measured charge pump operation is shown in Fig. 32.4.2, with the HOLD functionality ensuring minimal clock-switching related interference coupling into the CMUT once the desired bias voltage has been set. Two auxiliary clocks, φ_3 and φ_4, also provide a controlled self-discharge path once RESET goes high to avoid any high-voltage transients that might occur if internal nodes were left floating during discharge. Transient measurements in Fig. 32.4.2, using a 100pF capacitive load, demonstrate that the charge pump achieves a wide output voltage range from 0.5 to 64V with a tunable V_{REF} providing fine-grained control (~0.3V) over the charge pump output voltage.

An ultra-low noise, high DR sensor interface for the CMUT array is required to achieve the lowest NEP for SNR-constrained cross-medium sensing. Unlike low-noise, immersion CMUT AFEs that typically use current sensing architectures [6], the low acoustic impedance of air (which translates to low CMUT resistance) makes it more power and noise efficient to use a voltage amplifying AFE for air-coupled CMUTs. Our AFE is a three-stage design (Fig. 32.4.1): a low-noise, fixed-gain voltage amplifier (FGA) followed by a variable gain amplifier (VGA), and an output buffer. Maintaining the high CMUT sensitivity requires a high-impedance AFE interface; we achieve this by canceling capacitance at the input via a programmable negative Miller capacitance that is generated using capacitor banks placed in a positive feedback loop as shown in Fig. 32.4.3. The limited gain-bandwidth product of the FGA results in Z_{IN} having an undesirable negative resistance which is compensated using a bank of resistors, R_{damp}, ensuring that Z_{NEG} is largely capacitive at frequencies of interest. All stages use a self-biased, inverter-input based OTA architecture [7] to achieve a high NEF while making the AFE robust to PVT variations. Measurement results show uniform gain across channels, programmable from 36 to 66dB and an in-band (50 to 90kHz) noise figure of 0.54dB with 202.8μW power consumption per channel.

Figure 32.4.4 shows the electro-mechanical and all-electrical equivalent circuit model of the CMUT. As a preliminary tuning knob, we use the programmable bias voltage from the charge pump to electronically tune the parallel resonance frequency, f_p, of the CMUT. When tuning the bias voltage (30 to 52V), CMUT impedance and pitch-catch measurements show a wide frequency range but have lower open-circuit sensitivities (V_{oc}) at low bias voltages due to a loss in electro-mechanical conversion efficiency. To overcome this shortcoming, we devise a second frequency tuning mechanism that allows us to keep the CMUT biased at high voltage for efficient electro-mechanical conversion, while using the negative capacitance generated at the AFE input to tune the parallel resonance frequency. Unlike traditional equalization strategies that utilize negative capacitances, in addition to the parasitics, we also cancel the sensor's active capacitance to generate large frequency shifts. By tuning the negative capacitance (0 to 58pF, 1pF granularity) we obtain a higher impedance as we cancel more of the CMUT capacitance, providing higher sensitivities at higher frequencies albeit with lower quality factors (due to imperfect R_{damp} compensation). These two tuning mechanisms can thus be used to provide a synthesized frequency range >20× wider than the intrinsic CMUT bandwidth.

To demonstrate the water-to-air US uplink, a QPSK-modulated OFDM scheme is used with a hydrophone (RESON TC 4034) in a water tank serving as the US transmitter and the CMUT receiver array and chip placed at a standoff in air as illustrated in Fig. 32.4.5. Each element in the array (7 elements instead of 8, due to device damage) was configured to operate at a different orthogonal frequency by applying an optimal combination of bias voltage and negative capacitance, obtaining uniform sensitivity and bandwidth across the frequency range as seen in the pitch-catch measurement. The OFDM signal was transmitted with a pilot as shown schematically in the table. The data obtained across the CMUT elements was then summed, equalized, and successfully demodulated achieving a 28kb/s data rate with a BER of 3.3×10^{-5} at 10dB SNR.

In Figure 32.4.6, we compare our work to other approaches for acoustic communication across the water-air interface as well as in a single medium (air, water, and tissue). To perform a fair comparison, we use an Air-Adjusted NEP as a normalized metric for system sensitivity that is independent of sensing medium, transmitted pressure as well as propagation distance. We outperform other cross-medium acoustic communication approaches in both data rate (4.67×) and NEP (>1000×), while obtaining comparable data-rates to single medium communication systems with >100× better Air-Adjusted NEP indicating that the proposed system could also be deployed for long-range in-air acoustic communication and non-contact tissue-air communication for implants that use US data links. Photos of the chip die fabricated in a 180nm HV BCD process, packaged CMUT array, and a chip performance summary are shown in Fig. 32.4.7.

Acknowledgement:
The authors thank Prof. Khuri-Yakub and Dr. Bo Ma for providing the CMUT array, Mentor Graphics for the use of the Analog FastSPICE (AFS) Platform, as well as Ahmed Sawaby, Ernest So, and Max Wang for valuable discussions. Chip fabrication was made possible by the TSMC University Shuttle Program. This material is based upon work supported by Advanced Research Projects Agency-Energy Grant DE-AR0000825.

References:
[1] F.A. Blackmon, et al., "Experimental Detection and Reception Performance for Uplink Underwater Acoustic Communication Using a Remote, In-Air, Acousto-Optic Sensor," *IEEE J. Ocean. Eng.*, vol. 31, no. 1, pp. 179-187, 2006.
[2] F. Tonolini, et al., "Networking Across Boundaries: Enabling Wireless Communication Through the Water-Air Interface," *Proc. SIGCOMM*, pp. 117–131, 2018.
[3] B. Ma, et al., "Wide Bandwidth and Low Driving Voltage Vented CMUTs for Airborne Applications," *IEEE Trans. Ultrason. Ferroelectr. Freq. Control*, vol. 66, no. 11, pp. 1777–1785, 2019.
[4] G. Palumbo, et al., "Charge Pump Circuits With Only Capacitive Loads: Optimized Design," *IEEE TCAS-II*, vol. 53, no. 2, pp. 128–132, 2006.
[5] Y. Ismail, et al., "A 34V Charge Pump in 65nm Bulk CMOS Technology," *ISSCC Dig. Tech. Papers*, pp. 408–409, Feb. 2014.
[6] E. Kang, et al., "A 2pA/√ Hz Transimpedance Amplifier for Miniature Ultrasound Probes with 36dB Continuous-Time Gain Compensation," *ISSCC Dig. Tech. Papers*, pp. 354-355, Feb. 2020.
[7] M. Bazes, "Two Novel Fully Complementary Self-Biased CMOS Differential Amplifiers," *IEEE JSSC*, vol. 26, no. 2, pp. 165–168, 1991.

2022 IEEE International Solid-State Circuits Conference (ISSCC) | 978-1-6654-2800-2/22/$31.00 ©2022 IEEE | DOI: 10.1109/ISSCC42614.2022.9731648

Authorized licensed use limited to: Stanford University. Downloaded on March 27,2022 at 16:53:09 UTC from IEEE Xplore. Restrictions apply.

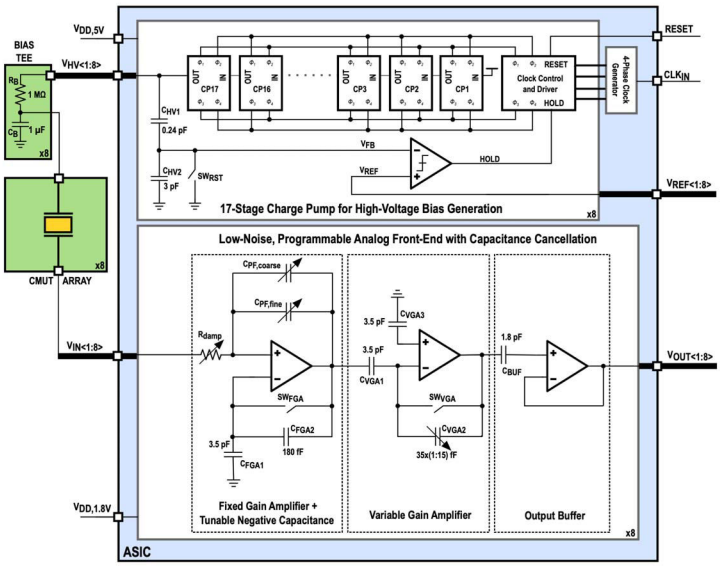

Figure 32.4.1: System block diagram with CMUT array and ASIC with programmable 8-channel charge pump and analog front-end.

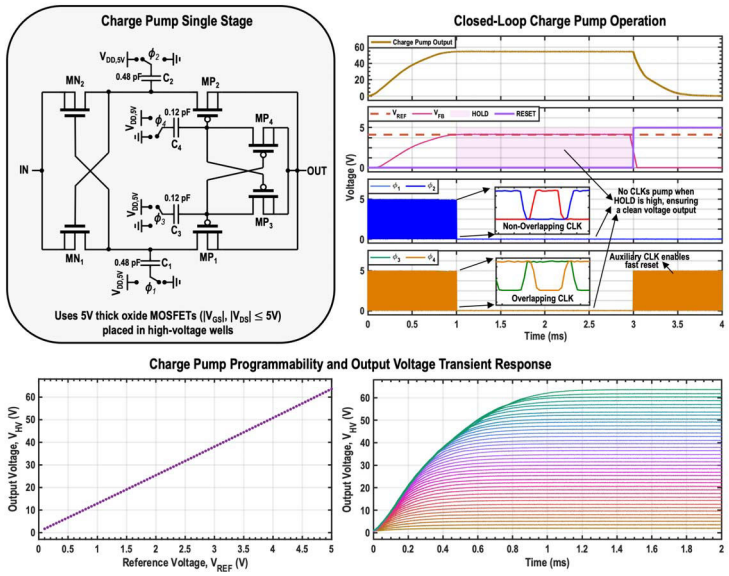

Figure 32.4.2: 4-phase charge pump stage; closed-loop charge pump measurement; programmable charge pump transient measurement.

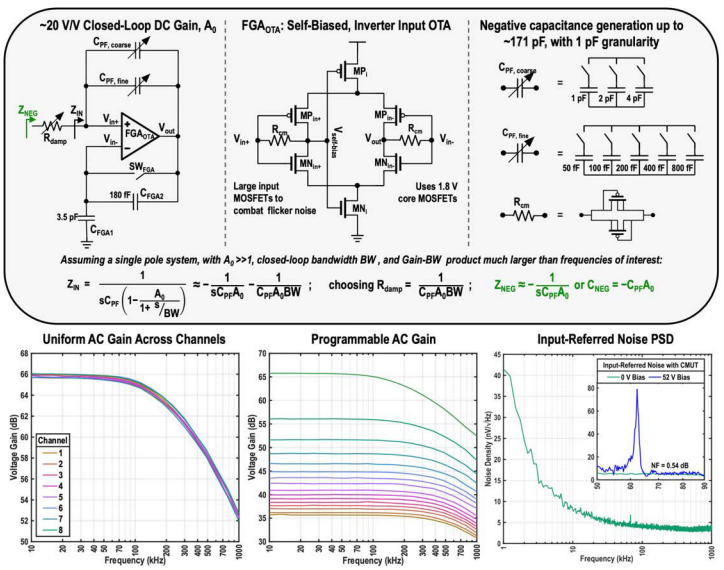

Figure 32.4.3: AFE first-stage schematic; programmable AC gain measurements; input-referred noise density measurement.

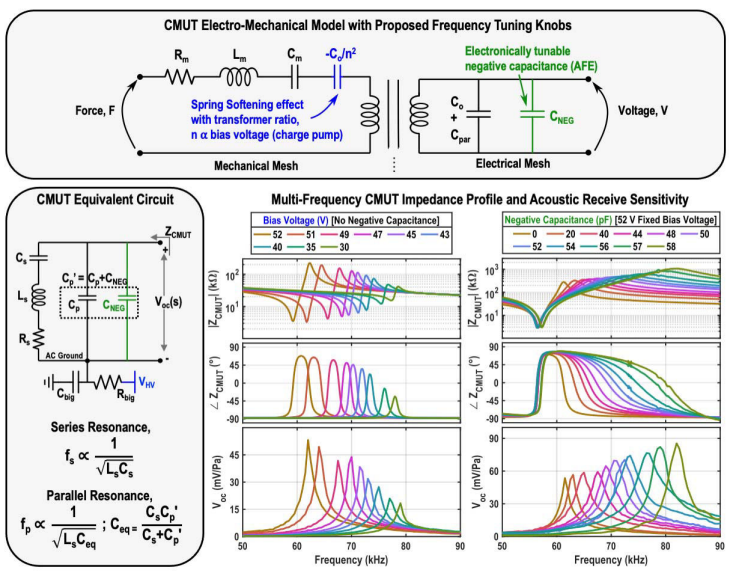

Figure 32.4.4: CMUT models with bias voltage and negative capacitance tuning; electrical impedance and airborne acoustic pitch-catch measurements.

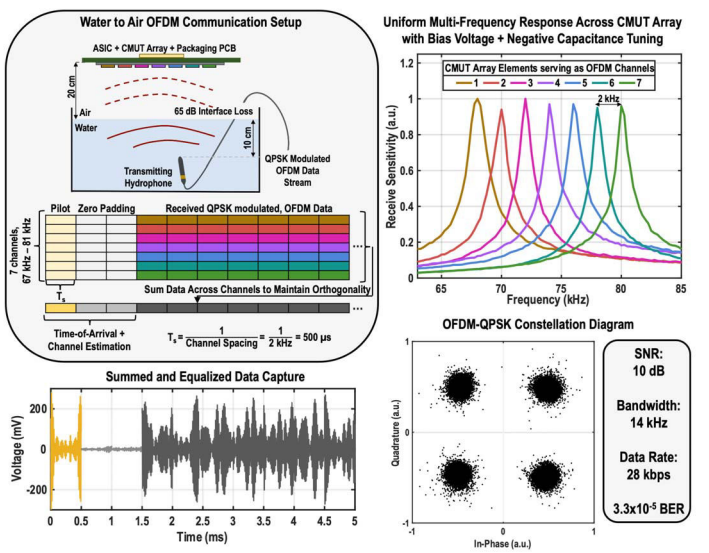

Figure 32.4.5: Experimental setup and measurements for cross-medium OFDM communication using the multi-frequency CMUT array.

	This Work	[1]	[2]	[8]	[9]	[10]
Acoustic Communication						
Medium	Communication Across Boundaries			Single-Medium Communication		
	Water-Air	Water-Air	Water-Air	Air-only	Water-only	Tissue-only
Modulation Scheme	OFDM (QPSK)	FSK	OFDM (QPSK)	OFDM (QPSK/16-QAM)	OFDM (BPSK)	OOK
# Sub-Carriers	7	N/A	64	45	-	N/A
Center Frequency	74 kHz	10 kHz	150 Hz	77 kHz	700 kHz	2.5 MHz
Bandwidth	14 kHz	5 kHz	100 Hz	45 kHz	200 kHz	100 kHz
Data Rate	28 kbps	6 kbps	200 bps	90 kbps / 180 kbps	-	95 kbps
BER (at SNR = 10 dB)	$3.3x10^{-5}$	-	10^{-2}	10^{-4} / 10^{-1}	10^{-2}	10^{-4} (SNR = 16 dB)
Sensor						
Sensor Type	Capacitive Micromachined Ultrasonic Transducer	Laser Doppler Vibrometer	mm-Wave radar	Electrostatic Ultrasonic Transducer	Piezoelectric Micromachined Ultrasonic Transducer	Piezoelectric Ultrasonic Transducer
Open Circuit Sensitivity (mV/Pa)	> 50	-	-	8	0.1259†	0.0119#
NEP (mPa/√Hz)	0.0018	1000	140000	0.23**	-	83.41#
Air-Adjusted NEP* (mPa/√Hz)	0.0018	16.73	2342.65	0.23	-	1.395

[8] W. Jiang et. al, T-UFFC, 64 (9), 2017; ** Experimentally measured by ourselves in the lab
[9] B. Herrera et. al, JMEMS, 29(5), 2020 ; † from F. Pop et. al, IEEE IFCS-ISAF, 2020 which uses the same sensor
[10] T.C Chang et. al, paper 27.7 ISSCC 2017; # Obtained by author correspondence
* Air-Adjusted NEP = NEP. $\sqrt{Z_{air}/Z_{sensing}}$ where $Z_{sensing}$ is the acoustic impedance in the sensing medium and mechanical noise floor $\propto \sqrt{Z}$

Figure 32.4.6: Comparison with state-of-the-art solutions for cross-medium acoustic communication in air and across different media.

Authorized licensed use limited to: Stanford University. Downloaded on March 27,2022 at 16:53:09 UTC from IEEE Xplore. Restrictions apply.

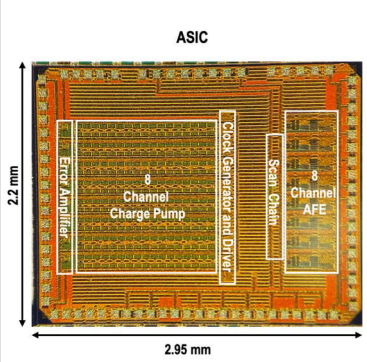

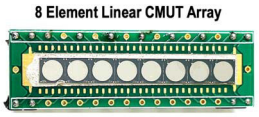

Process	180 nm 1P6M HV-BCD	
Die Size	2.2 x 2.95 mm²	
Charge Pump	Supply Voltage	5 V
	Programmable Output Voltage	0.5 V - 64 V (0.3 V granularity)
	Load Capacitance	100 pF
	CLK Frequency	2 MHz
	Rise Time	1.16 ms (for 64 V)
Analog Front-End	Supply Voltage	1.8 V
	Programmable Voltage Gain	36 dB - 66 dB
	Bandwidth	210 kHz - 740 kHz
	Dynamic Range	78 dB
	Power/channel	202.8 µW
	Minimum Detectable Pressure	59.7 µPa
	NEF' †	0.81 $\mu Pa.\sqrt{mW/Hz}$
	Negative Capacitance Range	1 pF - 171 pF (1 pF Granularity)
CMUT Array (variation across array elements)	Array Size	4 x 32 mm²
	Maximum Bias Voltage	60 V - 70 V
	Active Capacitance	57 pF - 65 pF
	Resonance Frequency (at 95% of Pull-In Voltage)	59 kHz - 62 kHz
	Operational Frequency Range (with Bias + Capacitance Tuning)	59 kHz - 82 kHz

† NEF' = $NEP.\sqrt{Power}$; metric from [6]

Figure 32.4.7: Chip micrograph; packaged 8-element CMUT array; measured chip and sensor performance summary.

978-1-6654-2800-2/22/$31.00 ©2022 IEEE
Authorized licensed use limited to: Stanford University. Downloaded on March 27,2022 at 16:53:09 UTC from IEEE Xplore. Restrictions apply.